https://doi.org/10.5194/egusphere-2026-4481
Preprint. Discussion started: 6 August 2026

Correction for above-clouds aerosols in geostationary satellite cloud property retrievals

Martin de Graaf[1], Ping Wang[1], Nikos Benas[1], and Jan Fokke Meirink[1]

[1]R&D Satellite Observations Department, Royal Netherlands Meteorological Institute (KNMI), De Bilt, The Netherlands

Correspondence: M. de Graaf, Royal Netherlands Meteorological Institute, R&D Satellite Observations, Utrechtseweg 297, De Bilt, The Netherlands, martin.de.graaf@knmi.nl

Abstract. The high-temporal-resolution observations from Spinning Enhanced Visible and InfraRed Imagers (SEVIRI) and its successor Flexible Combined Imager (FCI) of cloud optical thickness (COT) and cloud particle effective radius (CER), suffer from biases due to absorption by aerosols, when smoke is overlying the cloud scene. This is often the case over the south-east Atlantic Ocean (SEAO), which is an important part of the field of view of these instruments, which are onboard the geostationary Meteosat satellites series, stationed around 0^o latitude and longitude. The SEAO is an important area to study the impact of smoke on clouds, because the semi-permanent stratocumulus cloud decks over the dark ocean effectively reflect solar radiation and have a strong cooling effect on the Earth climate system. During the annual dry seasons in Africa, smoke from vegetation fires is advected over the clouds over the SEAO and mixes with them, making this region a natural laboratory to study aerosol-cloud-radiation interactions. In this paper, the biases in the COT and CER are quantified for typical smoke over cloud scenes, using an adaptation of the traditional cloud retrieval algorithms, including an extra channel in the usual bispectral minimisation procedure. This allows the simultaneous retrieval of COT, CER and above-cloud aerosol optical thickness (ACA AOT), which has been shown in several papers. The impact of smoke on the SEVIRI retrievals was investigated during July - October 2017 for a small region of the SEAO in the satellite field of view. The SEVIRI COT and CER were increased by a factor of 1.9 and 1.4, respectively, as a result of accounting for overlying smoke during two days with an average ACA AOT (550 nm) of 0.82. A similar event in 2025 during one day saw an increase in FCI COT and CER of 2.2 and 1.3, respectively, for an average ACA AOT of 0.95. Furthermore, the distribution of COT changed significantly when accounting for the overlying aerosols, showing a much wider distribution of COT values.

1 Introduction

Long-term satellite observations of clouds are indispensable for a range of applications, including climate monitoring, model evaluation and cloud process studies. The European Organisation for the Exploitation of Meteorological Satellites (EUMETSAT) Satellite Application Facility on Climate Monitoring (CM SAF) is dedicated to developing, generating, archiving and

https://doi.org/10.5194/egusphere-2026-4481
Preprint. Discussion started: 6 August 2026

distributing high-quality satellite-derived products of the global energy & water cycle and related sustained services in support of understanding our climate. One service is the operation of geostationary satellites over Africa and Europe, and generating accurate cloud property information for climate monitoring. The main instruments providing geostationary cloud products are SEVIRI onboard the Meteosat Second Generation (MSG) geostationary satellites series, and FCI onboard the Meteosat Third Generation - Imager(MTG-I) satellite series.

A prominent region in the geostationary satellites' field of view is the SEAO, characterised by extensive low cloud cover due to low sea surface temperatures (SST) from upwelling deep water near the coast. The cold, wet ocean surface encourages the formation of large stratocumulus decks at the top of the marine boundary layer (MBL) (e.g. Paluch and Lenschow, 1991). The free troposphere, on the other hand, is characterised by subsidence of warm clear air under the influence of the downward branches of the Hadley and Walker circulations, topping the boundary layer (Stevens, 2005). The result is a persistent cloud deck, sustained by moisture from the ocean and longwave cooling at the top of the layer, with a strong temperature inversion which the cumulus clouds are generally unable to penetrate. The moist, well-mixed MBL is characterised by a diurnal cycle in the stratocumulus cloud deck of thickening during the night and thinning during daylight hours as the sun evaporates cloud droplets. Stable south-easterly trade winds transport the stratocumulus clouds equator-ward, transforming the cloud deck into trade-wind shallow cumulus near the equator (e.g. Bretherton and Wyant, 1997; Wyant et al., 1997). The persistent stratus and trade-wind cumulus regimes are important temperature regulators, cooling the Earth's surface and boundary layer by reflecting sunlight over the dark ocean in the tropics (Randall et al., 1984; Albrecht et al., 1988).

During the monsoonal dry season in southern Africa, vegetation fires produce extensive smoke plumes reaching the free troposphere (de Graaf et al., 2010; Zuidema et al., 2018). Anticyclonic circulation over southern Africa favours the transportation of the smoke particles in the warm, free troposphere to the SEAO (Garstang et al., 1996; Swap et al., 1996). The absorption of sunlight by the smoke particles can increase the temperature inversion over the MBL, stabilising the cloud layer (Johnson et al., 2004; Yamaguchi et al., 2015). However, if the smoke is mixed within the MBL, the inversion may be weakened (Painemal et al., 2014; Rajapakshe et al., 2017), while the aerosol particles may act as condensation nuclei (Twomey, 1977; Diamond et al., 2018). Both processes change the stability of the cloud layer and affect the cloud fraction and radiative effects in the region (Xue and Feingold, 2006; Zhou et al., 2017; Ajoku et al., 2021).

These aerosol-cloud-radiation interactions are among the least understood processes and form the largest uncertainties in general circulation models (GCMs) (Forster et al., 2023). Especially over the SEAO region large differences were found between GCMs in aerosol effects and aerosol forcings. A comparison of 16 GCMs participating in AEROCOM simulating the direct radiative forcing over the SEAO showed that the models differ in magnitude and even sign of the forcing (Myhre et al., 2013; Haywood et al., 2021). In order to accurately model the aerosol direct effect, models need to represent both the aerosol micro- and macrophysical properties and geographic distribution, and the cloud geographic distribution, cloud fraction, cloud liquid water content, cloud vertical profile and cloud particle effective radii (Keil and Haywood, 2003).

Therefore, for monitoring purposes and science applications it is imperative that satellite retrievals of cloud properties are of high accuracy. In the SEVIRI and FCI cloud retrieval applications, cloud optical thickness (COT) and cloud particle effective radius (CER) are retrieved using the common bi-spectral (visible–shortwave infrared, VIS–SWIR) LookUp Table

https://doi.org/10.5194/egusphere-2026-4481
Preprint. Discussion started: 6 August 2026

(LUT) approach developed by Nakajima and King (1990). Aerosols are not considered in these retrievals, and it is well-known that the resulting COT and CER are biased if absorbing aerosols are present above the clouds (Haywood et al., 2004). In the current study, an approach pioneered by Peers et al. (2019) is evaluated, taking the presence of aerosols into account in the inversion of the cloud parameters, using measurements at three channels, two in the SWIR and one in the VIS, to account for the absorption of radiation by aerosols. The effect of the aerosols on the retrieved COT and CER is quantified in this paper.

In the next section, the upgraded retrieval algorithm is introduced. It closely follows Peers et al. (2019) and yields an above-cloud aerosol optical thickness (ACA AOT), cloud optical thickness (ACA COT) and cloud particle effective radius (ACA CER) product. The bias in cloud properties due to not accounting for absorbing aerosols is quantified in section 3 for the African biomass burning season in 2017, which is well documented. The ACA products are compared to various additional measurements of above-cloud aerosols in section 4, like modelled aerosol distributions from the Copernicus Atmosphere Monitoring Service (CAMS) and the Absorbing Aerosol Index (AAI) from Global Ozone Monitoring Experiment-2 (GOME-2). Then, results from the application of the current algorithm to the new FCI instrument are shown in section 5. Finally, the implication of the cloud parameter bias for climate monitoring and the way forward using additional capabilities of FCI compared to SEVIRI is discussed in section 6.

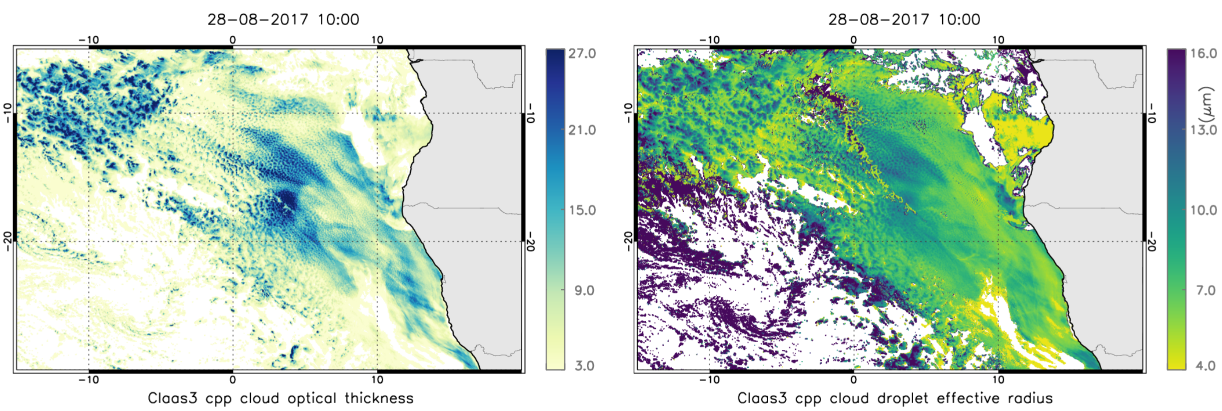

Figure 1. CLAAS-3 COT and CER retrievals over the SEAO on 28 Aug. 2017 at 10:00 UTC.

2 Data and methods

2.1 SEVIRI

SEVIRI is a series of imager instruments on the MSG geostationary satellites Meteosat-8, 9, 10 and 11, operated by EUMETSAT, which have been operational in the period from January 2004 to present. Apart from one high-resolution visible (HRV) channel, SEVIRI carries 11 channels between 0.6 and 14 μm with a resolution of 3×3 km^2 at nadir and a 15 minute full disk repeat cycle. SEVIRI is not equipped with an on-board calibration device for these channels. The reflectances in the SEVIRI

https://doi.org/10.5194/egusphere-2026-4481
Preprint. Discussion started: 6 August 2026

Level-1.5 data files were recalibrated with respect to Aqua/MODIS following the approach presented in Meirink et al. (2013). The reflectance R at wavelength λ is defined by:

$$R(\lambda) = \frac{\pi I(\lambda)}{\cos(\theta_0) \cdot E_0(\lambda)}, \quad (1)$$

where, in the ultra-violet (UV) and VIS, $I(\lambda)$ is the radiance reflected by the Earth (atmosphere and surface) to the sensor, θ_0 is the solar zenith angle and $E_0(\lambda)$ is the solar irradiance.

2.2 MSG and MTG Cloud physical products

The 'CM SAF cLoud dAtAset using SEVIRI' (CLAAS) series of cloud property climate data records produced by the CM SAF have a coverage centred over Africa and the Atlantic Ocean (Stengel et al., 2014; Benas et al., 2017). The third edition (CLAAS-3, (Meirink et al., 2022)) was published in December 2022 (Benas et al., 2023). It contains cloud physical properties (CPP), such as a (probabilistic) cloud mask, cloud top height, cloud thermodynamic phase, and a set of cloud optical and microphysical properties. The latter include cloud optical thickness (COT), cloud particle effective radius (CER), liquid and ice water path (LWP/IWP), as well as liquid cloud droplet number concentration and geometrical thickness.

In the CLAAS-3 retrievals 0.64 μm is used for COT retrieval and either 1.6 or 3.9 μm for CER. Throughout this paper, only the CPP properties determined at 0.64 and 1.6 μm will be used. Note that the effect of aerosol absorption may be smaller for the 3.9 μm channel. Example retrievals from CLAAS-3 are presented in Fig. 1. The COT in figures and results is reported at 0.64 μm, although a wavelength specification is not given, because the reflectance of a liquid cloud is almost spectrally flat from the UV to the near-infrared (NIR).

In the next edition of CM SAF CPP, CLAAS-4, MTG FCI observations will be added.

2.3 Above-cloud aerosol and alternative cloud retrieval algorithm

To account for the aerosol absorption, the retrievals were modified to simultaneously retrieve ACA AOT with the COT and CER, by adding a third channel at 0.82 μm. The absorption by small particles is strongly wavelength-dependent (de Graaf et al., 2012) and the presence of absorbing aerosols above clouds modifies the apparent colour of the clouds, especially in the UV-VIS.

LUTs were prepared of simulated reflectances at 0.64 μm, 0.82 μm and 1.63 μm for scenes with liquid clouds and aerosols above the clouds. One kilometre thick clouds were placed between 0–1 km altitude, while a one kilometre thick aerosol layer was present between 2–3 km altitude. Simulations were performed for AOT between 0 – 1.5 (at 0.64 μm), COT between 0 and 256, and CER between 3 and 34 μm, using the KNMI Radiative Transfer Model (RTM) Doubling-Adding KNMI (DAK) (De Haan et al., 1987; Stammes, 2001). Details of the aerosol and cloud properties used in the simulations are listed in Table 1. The LUTs differ from the operational CLAAS-3 LUTs, which were generated using the same RTM DAK but without aerosols. The aerosol model is the same as used in Peers et al. (2019), which is based on the microphysical properties derived from *in situ* measurements during the CLARIFY-2017 aircraft campaign (Haywood et al., 2021). During this campaign the Facility for

https://doi.org/10.5194/egusphere-2026-4481
Preprint. Discussion started: 6 August 2026

Airborne Atmospheric Measurements (FAAM) BAe 146 aircraft was deployed from Ascension Island in August and September 2017, with the main objective of studying biomass burning aerosol interactions with both radiation and clouds over the SEAO.

The spectral contrast created by aerosol overlying clouds is shown in Figure 2 using the simulated reflectances at the SEVIRI VIS-SWIR channels. In panel (a) the ratio of the reflectance at 0.64 μm and 0.82 μm is plotted as a function of the reflectance at 0.82 μm, for simulated cases of absorbing aerosols above clouds over an ocean surface with varying AOT and COT, and a CER of 10 μm.

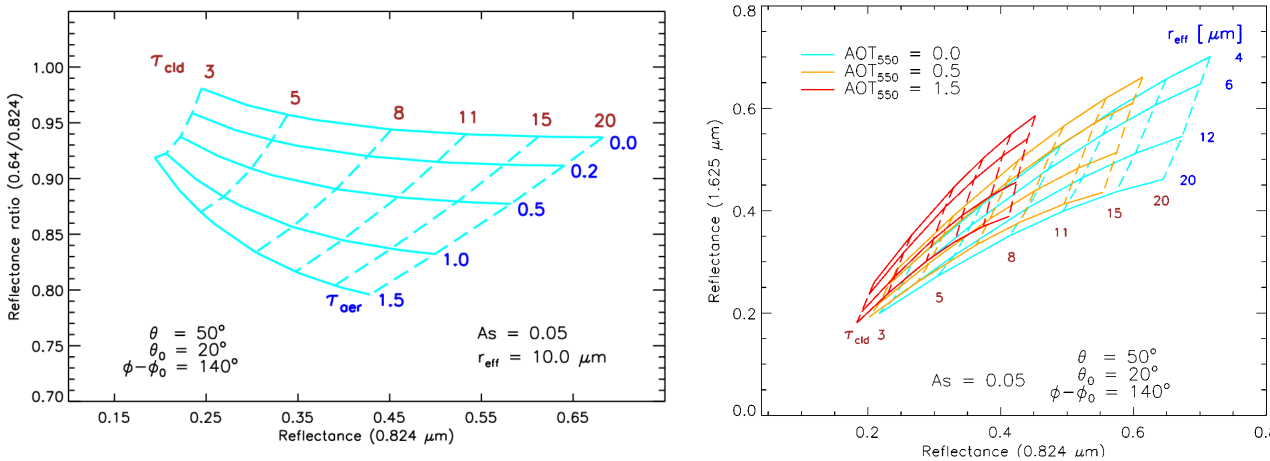

Figure 2. (left) Lines of equal τ_{aer} and τ_{cld} in a diagram of reflectance ratio $R_{0.64}/R_{0.82}$ as a function of the reflectance at 0.82 μm for absorbing aerosols above clouds; (right) Lines of equal τ_{cld} and r_{eff} in a diagram of reflectances at 0.82 μm and 1.6 μm for clouds without (blue) and with (orange and red) aerosols above. The viewing zenith angle for the simulated cases was 50°, the solar zenith angle was 20°, and the relative azimuth angle 140°. See Table 1 for the smoke and clod droplet properties. A Lambertian surface with an albedo of 0.05 was assumed.

In panel (b) the reflectance at 1.6 μm is plotted as a function of the reflectance at 0.82 μm for varying COT and CER, for several values of the AOT (at 550 nm) of simulated cases of aerosols above clouds over an ocean surface, showing the retrieval principle of the cloud parameters. For some combination of measured reflectances, the COT and CER can be retrieved from a LUT of these simulations. In orange and red the same combination of reflectances is shown, affected by the light absorption from the overlying aerosols. Clearly, if the measured TOA reflectance is lower than anticipated, the retrieved COT and CER will be biased. When the AOT is retrieved simultaneously, the bias in the COT and CER will be reduced.

The spectrally broad SEVIRI channels include light absorption by several atmospheric gases which must be corrected for before comparison with the LUT nodes is possible. The applied atmospheric correction was the same as for the CLAAS-3 retrieval (but for three channels), requiring the water vapour path, total ozone column, cloud top height and (geometrical) air mass factor as input. The same method was applied here for all retrievals, using ECMWF Re-Analysis 5 (ERA5) water vapour and ozone fields, and cloud top height and airmass factor from the CLAAS-3 products.

https://doi.org/10.5194/egusphere-2026-4481
Preprint. Discussion started: 6 August 2026

Three datasets are considered: (1) COT and CER retrievals from the CLAAS-3 algorithm, (2) ACA AOT, ACA COT and ACA CER from the algorithm described here, and (3) COT and CER retrieved with the algorithm from this paper but with ACA AOT fixed at zero. The latter dataset is called CPP after the CLAAS-3 Cloud Physical Properties retrieval algorithm. The CPP retrieval allows a better quantification of the aerosol effects on the cloud parameters, eliminating any algorithm differences between the CLAAS-3 retrievals and the CPP retrievals, even though the differences between the CLAAS-3 COT and CER, and the CPP COT and CER are very small.

3 Results

Four months of SEVIRI data from July – October 2017 were processed using the algorithm described above for a small section of the SEVIRI observation disc between $15-30°$S and 15°W–15°E. The total number of 3×3 km^2 pixels in this area is

Table 1. Size distribution parameters and optical properties of the aerosol and cloud models used to generate the Lookup Table. The following notations for aerosol properties are used: $r_{\text{fine}}/r_{\text{coarse}}$ are the geometric mean radii, $\sigma_{\text{fine}}/\sigma_{\text{coarse}}$ the standard deviations, and $N_{\text{fine}}/N_{\text{coarse}}$ the number fractions of the fine/coarse mode; g is the asymmetry factor and ω_0 the single scattering albedo. Water refractive index from Segelstein (1981).

	Aerosol model			
Size distribution	Bimodel lognormal distribution			
	r_{fine} = 0.12 μm	σ_{fine} = 1.42		N_{fine}= 0.9996
	r_{coarse} = 0.62 μm	σ_{coarse} = 2.23		N_{coarse} = 0.0004
Refractive index	1.51 - 0.029i			
Wavelength	0.55 μm	0.64 μm	0.82 μm	1.63 μm
ω_0	0.852	0.839	0.804	0.643
g	0.649	0.612	0.538	0.468
AOT (0.64μm)	0.0 0.2 0.5 1.0 1.5			
	Cloud model			
Wavelength	0.55 μm	0.64 μm	0.82 μm	1.63 μm
Refractive index	1.34-2.5·10^{-9}i	1.33-1.6·10^{-8}i	1.33-1.8·10^{-7}i	1.31-8.2·10^{-5}i
Size distribution	Gamma law distribution (ν_{eff} = 0.1 μm)			
CER [μm]	3.0 4.2 6.0 8.5 12.0 17.0 24.0 34.0			
COT	0.00 0.25 0.35 0.50 0.71 1.00 1.41 2.00 2.83 4.00 5.66 8.00 11.31 16.00 22.63 32.00 45.26 64.00 90.51 128.0 181.0 256.0			

https://doi.org/10.5194/egusphere-2026-4481
Preprint. Discussion started: 6 August 2026

1089×847 (~1M). The area is known to be severely affected by smoke from annual burning in Africa during the monsoonal dry season (e.g. Garstang et al., 1996). In 2017, the smoke from Africa was studied extensively during two aircraft campaigns from Ascension Island (Haywood et al., 2021) and Namibia (Redemann et al., 2020), and ground-based measurements on Ascension Island (Zuidema et al., 2018).

3.1 Retrieval of the ACA parameters

An example of the ACA retrieval is shown in Figure 3. The figure shows the situation on 28 Aug. 2017 as observed by Terra/MODIS at around 10:30 local time (LT) in the first panel. The typical extensive stratocumulus cloud deck over the SEAO can be seen, breaking up near the equator into shallow cumulus in a south-easterly flow. Near the coast and over the continent (especially in the north-east part of the picture), an extensive smoke plume can be seen as the grey haze over land and the dark colouring of the clouds. The other panels show the retrieved ACA AOT, ACA COT and ACA CER for this day and time. The AOT shows a strong gradient from the northeast to the southwest.

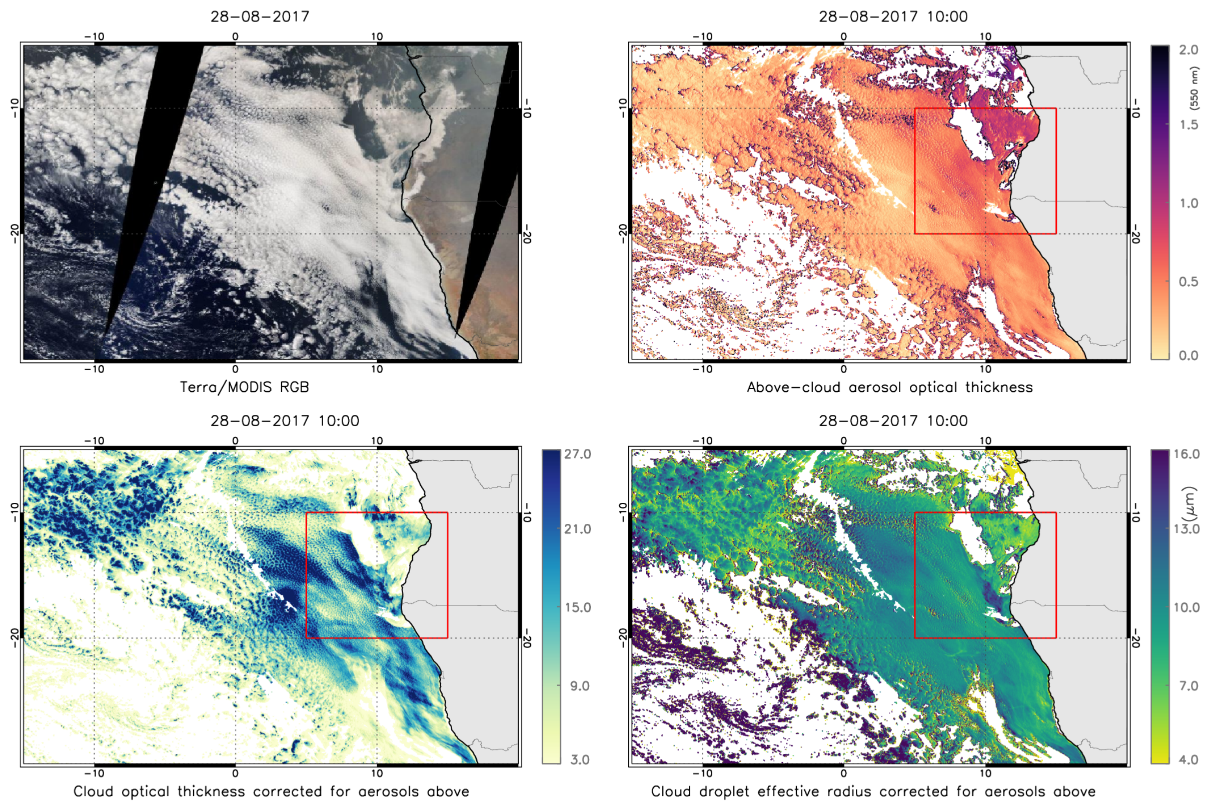

Figure 3. RGB image from Terra/MODIS, acquired around 10:30 local time, ACA aerosol optical thickness, ACA cloud optical thickness, and ACA cloud particle effective radius, on 28 Aug. 2017, 10:00 UTC.

https://doi.org/10.5194/egusphere-2026-4481
Preprint. Discussion started: 6 August 2026

The ACA COT and ACA CER can be compared to the CLAAS-3 retrievals from Figure 1. Clearly, both the ACA COT and ACA CER are higher than the CLAAS-3 COT and CER. This is due to the correction for the light-absorption by the aerosols over the clouds: less radiation is reflected back to the instrument, which is erroneously interpreted in the CLAAS-3 retrievals as a lower COT and also a lower CER, which is now corrected for in the new retrievals.

3.2 Correction of the cloud parameters for ACA

The differences due to the correction for aerosols overlying the clouds are illustrated in Figure 4, showing the difference between the CPP retrieval (for AOT=0) and the ACA COT and CER retrievals. Except near cloud edges, the COT and CER are always higher in the ACA retrieval and increase for increasing ACA AOT, especially for COT (as can be seen in the high AOT area in the northeast). The results near cloud edges and in inhomogenous cloud fields show large differences due to large uncertainties in inhomogenous data. Such results were removed in Peers et al. (2019), by aggregating the data onto a regular 0.125×0.125 degree grid and removing inhomogenous data, but this was not attempted here.

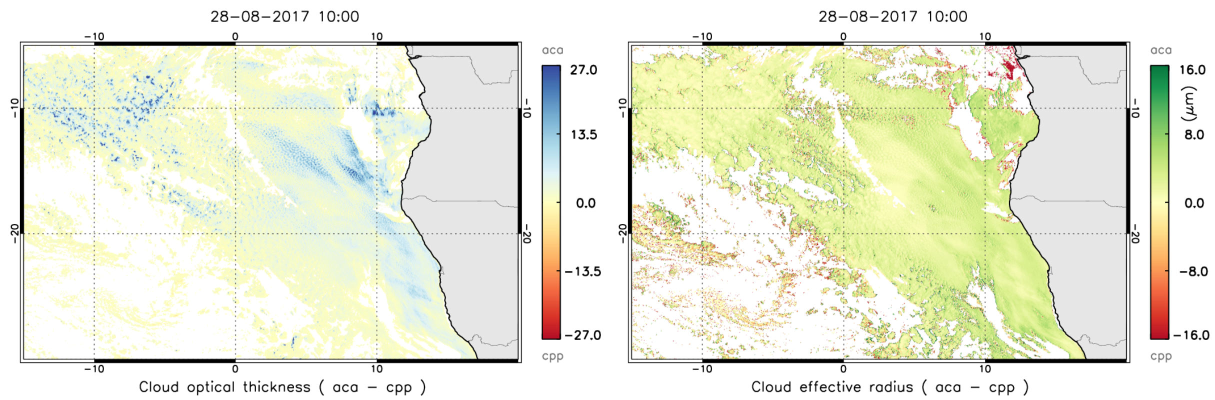

Figure 4. Difference between ACA and CPP cloud optical thickness, and ACA and CPP cloud particle effective radius, on 28 Aug. 2017, 10:00 UTC.

The effect of the smoke was analysed further using the area indicated in Figure 3 by the red square. In this region close to the coast, the ACA AOT peaked at the end of August and beginning of Sept. 2017, and it was selected to analyse the effect of the AOT on the cloud parameter retrievals. The diurnal cycle of the ACA AOT, COT and CER, averaged over the area, is shown in Figure 5 for 28 Aug. 2017 and 6 Sept. 2017, together with the CLAAS-3 COT and CER. The first panel shows the changes through the day for the retrievals in Figures 3 and 4, and the second can be compared directly to Figure 13 in Peers et al. (2019).

The retrievals during both days are comparable. The evolution of the retrieved ACA AOT is very stable during the day from about 07:30 until 15:00, after which the retrieval becomes uncertain due to mismatches between the measurements (at high solar zenith angles) and the modelled reflectances. Furthermore, some fluctuations can be observed in AOT (and the cloud parameters) around noon, 09:30 and between 14:00 and 15:00. These are related to the glory (noon) and cloud bow (9:30 and

https://doi.org/10.5194/egusphere-2026-4481
Preprint. Discussion started: 6 August 2026

14:30) features. The CLAAS-3 cloud parameters, in particular effective radius, are also affected by these issues, and have been analysed in Benas et al. (2019). Note that in the CLAAS-3 Level 2 data flags are present to identify retrievals for which the measurements are outside the LUT. The effective radii of the corresponding pixels are not included in the Level 3 products but are included in the averages in Figure 5.

Both the COT and CER are higher when corrected for the overlying aerosols, as before. The ACA COT retrievals show a stronger dependence on the geometry than the regular CLAAS-3 retrievals (before 10:00 and after 15:00). During these periods when the sun is low, the difference between the measurements and the plane-parallel LUT calculations becomes very large. Between 10:00 and 15:00 the COT is decreasing during the day, which is expected in this area, where clouds build up during the night, and the overhead sun burns away the clouds during the day.

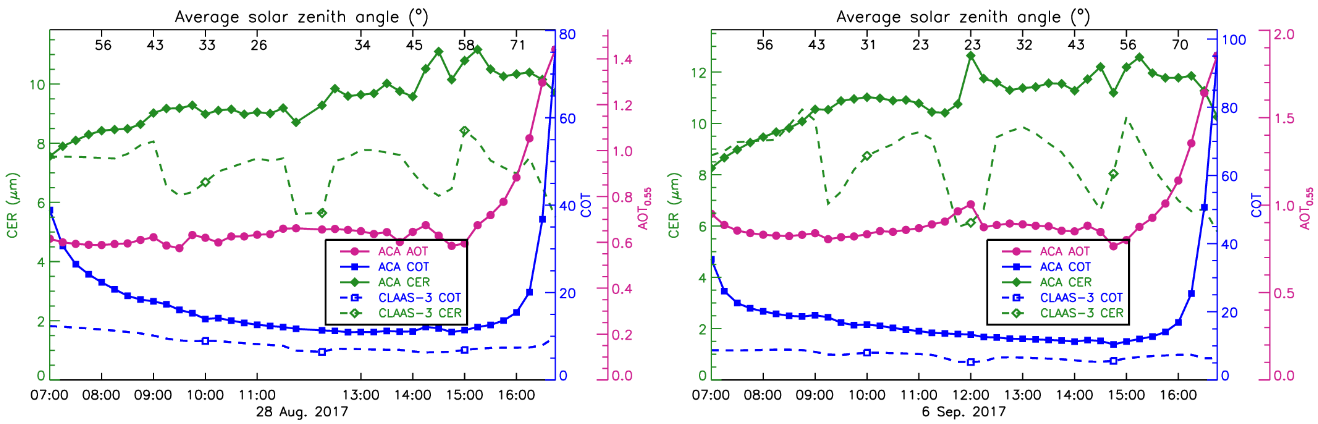

Figure 5. Diurnal cycle of the ACA AOT, COT and CER, and CLAAS-3 COT and CER on 28 Aug. and 6 Sept. 2017.

The difference between the ACA and CLAAS-3 COT and CER is illustrated further in Figure 6. For two days, 5 and 6 Sept. 2017, the ACA COT and CER were averaged over the selected area and compared to the averaged CLAAS-3 COT and CER. Only the retrievals between 10:00 and 15:00 were taken into account. The average ACA AOT at 0.55 μm for this period and region was 0.82. Clearly, the retrieved cloud optical thickness is increased when the overlying smoke is accounted for. The ACA COT was about 13, averaged over the entire period and region, while the CLAAS-3 average COT was 6.9. The increase was over the entire range of COT, but the distribution is changed from COT under 20 to a distribution of COT from 0 to 40. This is a significant change in cloud optical thickness. The CER was also increased in the ACA retrieval compared to the CLAAS-3 retrieval, on average, from 7.5 to 11 μm. The distribution for CER did not change much, but instead shifted to somewhat higher values.

3.2.1 Quantification of cloud parameter change for ACA

It is important to quantify the effect of the light absorption on the retrieval of the cloud parameters, to understand the uncertainties associated with overlying smoke. Of course, this is dependent on many factors, most notably the assumptions on the

https://doi.org/10.5194/egusphere-2026-4481
Preprint. Discussion started: 6 August 2026

aerosol refractive index. Here, a particular case of smoke was analysed during the ORACLES and CLARIFY flight campaigns, and the refractive index can be assumed to be relatively well characterised. The results from this case study are not necessarily applicable to other cases of smoke above clouds, and in general it cannot be said with certainty that the absorbing aerosols are smoke particles, but instead can be dust or pollution. Still, the change in cloud parameters was determined as a function of retrieved ACA AOT for this case, to show how smoke affects the cloud parameter retrievals. The results are illustrated in Figures 7–9.

In Fig. 7 the change $(c_{\mathrm{ACA}} - c_{\mathrm{CPP}})/(c_{\mathrm{ACA}} + c_{\mathrm{CPP}})$, where c is either COT or CER, is plotted as a function of the ACA AOT at two different times during 6 Sept. 2017, again for the measurements within the red rectangle in Fig. 3. The majority of the COT and CER retrievals are increased for higher AOT and the change is considerable. A relative change of 0.5 at an AOT of 1.0 means that the ACA retrievals are three times as large as the CPP retrievals, and the changes can be even larger than that. Furthermore, the increase is different at different times of the day. To quantify this, a linear least-squares fit was determined at each time. The point cloud does not exactly follow a straight line, but the linear fit parameters indicate the change in sensitivity of the cloud parameters to the retrieved ACA AOT.

To understand the changes that can be expected, the analysis was repeated with simulated reflectances from the ACA LUT, where c_{ACA} was determined for simulated AOT of 0, 0.2, 0.5, 1.0 and 1.5, COT values of 2.0, 4.0, 8.0, 16.0, 32.0, 64.0 and CER of 6.0, 12.0 and 24.0 at the viewing geometries of SEVIRI for the point 10°S, 10°E, which is in the middle of the smoke plumes. c_{CPP} is the corresponding cloud parameter at AOT=0. An example simulation and fit is shown for both COT and CER in Figure 8, which may be compared to the top panels in Fig. 7.

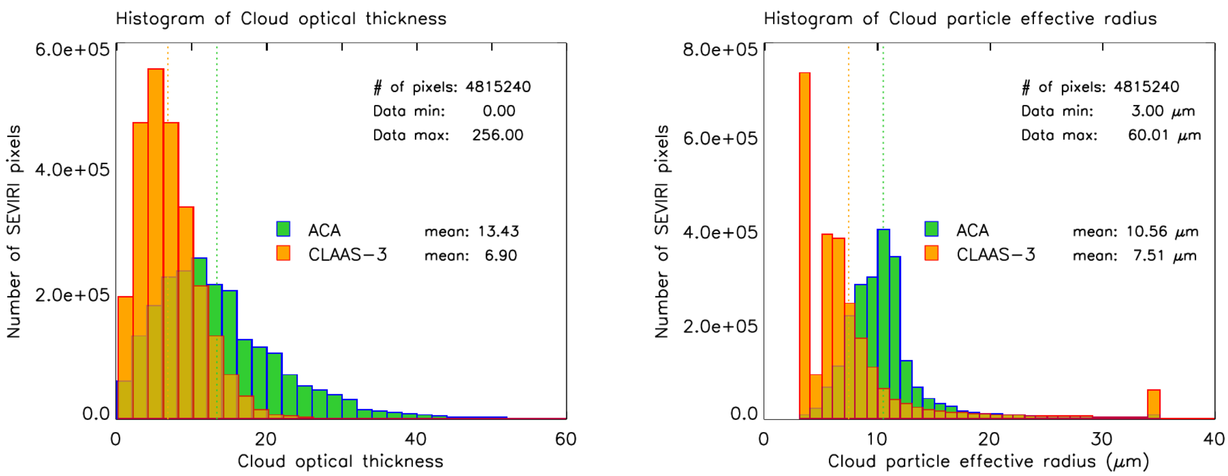

Figure 6. (Left panel) Histogram of the cloud optical thickness on 5 and 6 Sept. 2017 between 10:00–15:00, in the area between 10–20°S and 5–15°E, corrected for aerosols above the clouds (ACA; green) and the CLAAS-3 (orange) retrievals. (Right panel) Same as the left panel but for the cloud particle effective radius.

https://doi.org/10.5194/egusphere-2026-4481
Preprint. Discussion started: 6 August 2026

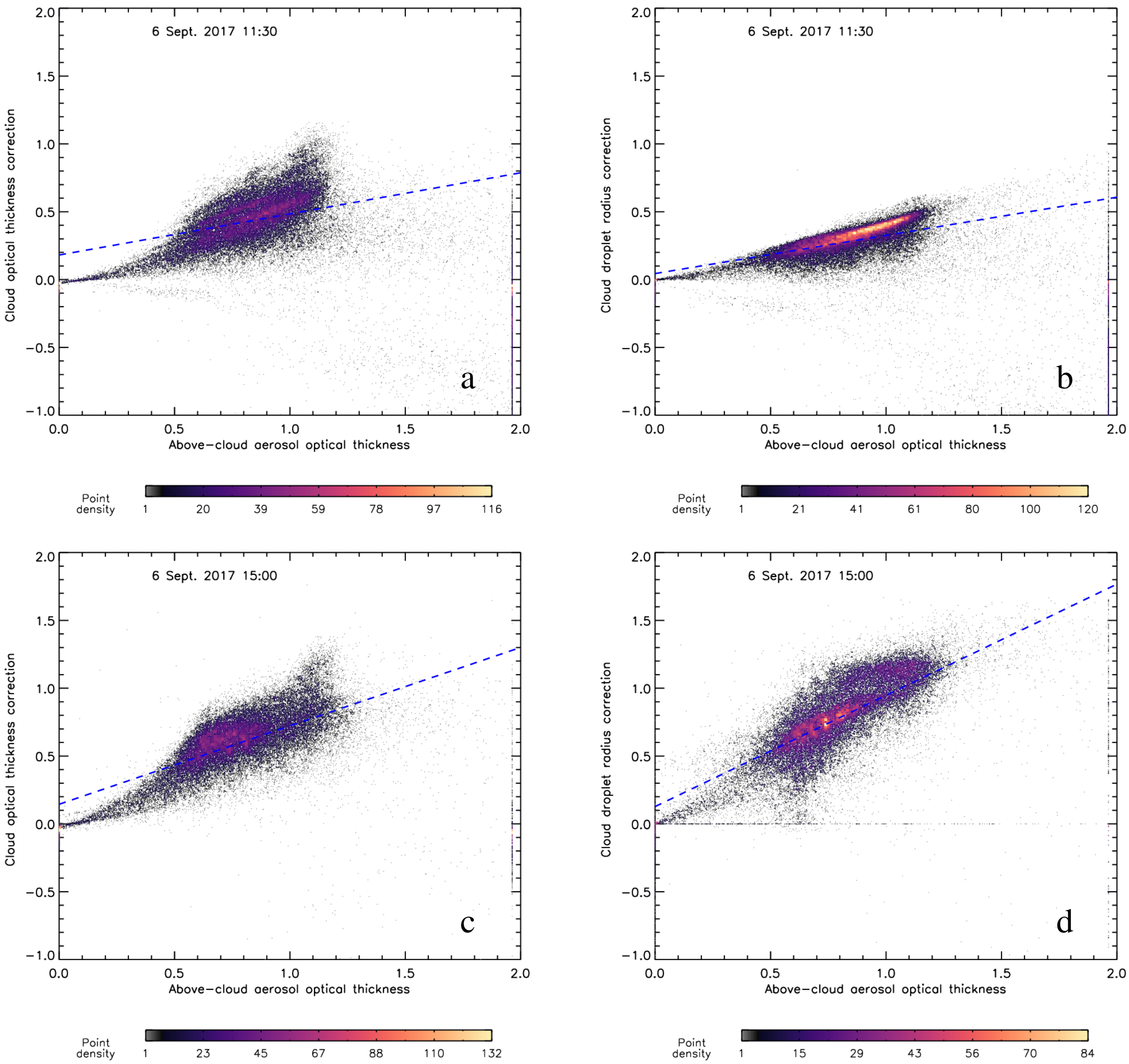

Figure 7. (a) Change of the cloud optical thickness corrected for aerosol above the cloud and uncorrected (COT_{ACA} - COT_{CPP})/(COT_{ACA} + COT_{CPP}) versus the optical thickness of the aerosols above the cloud (AOT_{ACA}) and (b) the change of the cloud particle effective radius corrected for aerosol above the cloud and uncorrected (CER_{ACA} - CER_{CPP})/(CER_{ACA} + CER_{CPP}) versus the optical thickness of the aerosols above the cloud (AOT_{ACA}) on 6 Sept. 2017 11:30. (c) and (d) same as (a) and (b) but at 15:00. The blue dashed lines shows linear least squares fits.

https://doi.org/10.5194/egusphere-2026-4481
Preprint. Discussion started: 6 August 2026

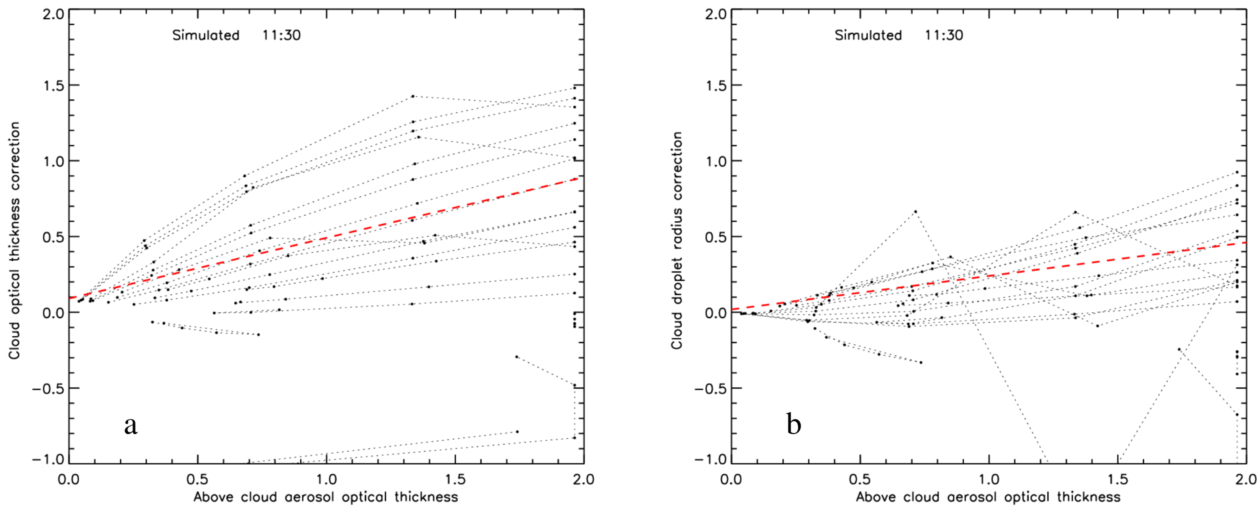

Figure 8. Change of the (a) simulated COT and (b) simulated CER, corrected for aerosol above the cloud and uncorrected (c_{ACA} - c_{CPP})/(c_{ACA} + c_{CPP}) versus the simulated AOT_{ACA} for a SEVIRI geometry at 10°S, 10°E, 11:30. The red line is a linear least squares fit.

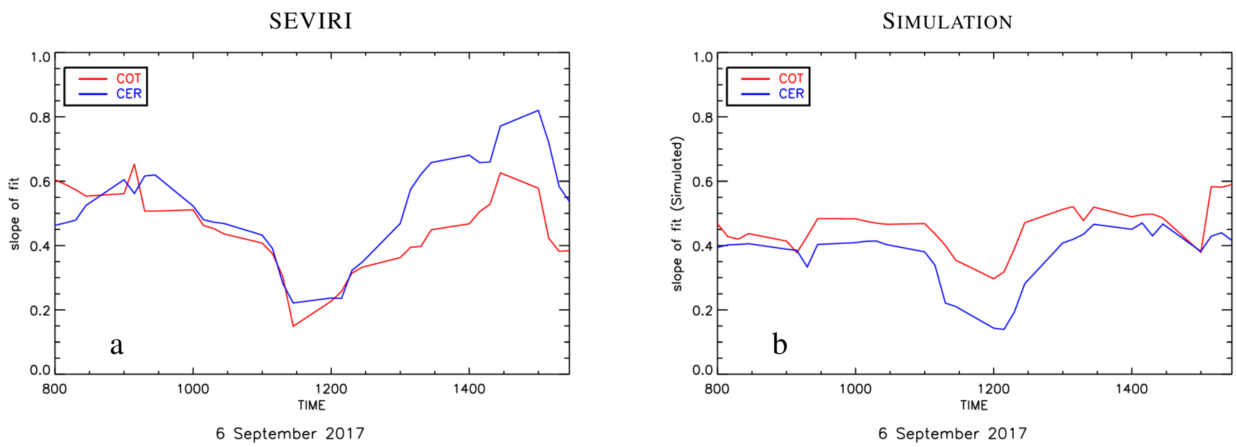

Figure 9. Diurnal cycle of the slope of the linear regression on the relative differences of the COT (red) and CER (blue) on 6 Sept. 2017 for (a) SEVIRI measurements as depicted in Fig. 7 and for (b) simulated reflectances as depicted in Fig. 8

The fits were determined at each time during the day of 6 Sept. 2017, for both the SEVIRI measurements and the simulations, and the slope to the fits are plotted in Figure 9. This figure gives an indication of the relative change of the COT and CER per unit AOT for the SEVIRI measurements (left panel, related to Fig. 7) and for the simulations (right panel, related to Fig. 8). The left panel shows that the sensitivity of the retrievals to AOT is large, from 0.2 to 0.6 for COT and up to 0.8 for CER. These high relative changes are probably due to increases of small values, as illustrated in Figure 6. The shift in CER is mainly from very small to higher values. COT is affected significantly by the light absorption of the smoke in both relative and absolute sense.

The right panel shows the sensitivity of the cloud parameters to AOT that may be expected theoretically with the smoke model that was used to build the ACA LUT. Clearly, the large sensitivity of around 0.4 to 0.5 for COT and CER are evident also from the simulations. The diurnal cycle in the simulated sensitivity to AOT is smaller than in the measurements, but the glory and cloud bow effects are represented well. Especially the glory has a large effect on both the CLAAS-3 and CPP retrievals.

The differences between the left and right panels of Figure 9 point to retrieval uncertainties due to the assumed aerosol model and limitation in the RTM. The RTM computes the light absorption by the aerosols using average and simplified assumptions for the aerosols and the clouds and a plane-parallel atmosphere. Even if the models are carefully determined, in reality the path of reflected light can be complicated and the model may not represent the aerosol effects accurately under different circumstances. The change in retrieved cloud parameters are larger than expected from the model simulations, showing that the model representation of the aerosols and clouds are not accurate enough to completely account for the light absorption by the aerosols for this case.

4 Comparison with reference products

In this section, the ACA AOT is compared with CAMS total AOT at 550 nm, available at a three hour temporal grid, and AAI from GOME-2B, available at the GOME-2 local overpass time of around 9:30 LT. Both indicate the presence of aerosols above clouds in independent and different ways, both with their own strengths and weaknesses. CAMS aerosols are distributed by a transport model independent of clouds, and can indicate the presence of both and therefore show the presence of aerosols above clouds. However, the aerosol concentrations are constrained with assimilated MODIS AOT observations, which are only performed in clear-sky scenes. The GOME-2B AAI observations, indicating absorption by UV-absorbing aerosols (like smoke) are equally valid in clear-sky and cloudy scenes, but the interpretation of the unitless and qualitative AAI is somewhat arbitrary and depends on the height of the aerosol layer, the AOT, single scattering albedo and asymmetry parameters of the aerosols, geometry, and wavelengths of the AAI, among others.

4.1 Comparison with CAMS model data

The ACA AOT within the red rectangle in Fig. 3 were averaged from 09:00 to 09:30 and compared to CAMS total AOT at 550 nm at 09:00 UTC, for all four months considered in this study. The result is shown in the top panel of Fig. 10. The comparison is remarkably good. Although in the first two months the ACA AOT is almost twice as high as the CAMS AOT, and sometimes a peak in one of the data series is missed in the other, the general trend is clearly the same. This is somewhat surprising for CAMS modelled data, which are constrained using clear-sky AOT observations from MODIS, and compared to SEVIRI ACA

https://doi.org/10.5194/egusphere-2026-4481
Preprint. Discussion started: 6 August 2026

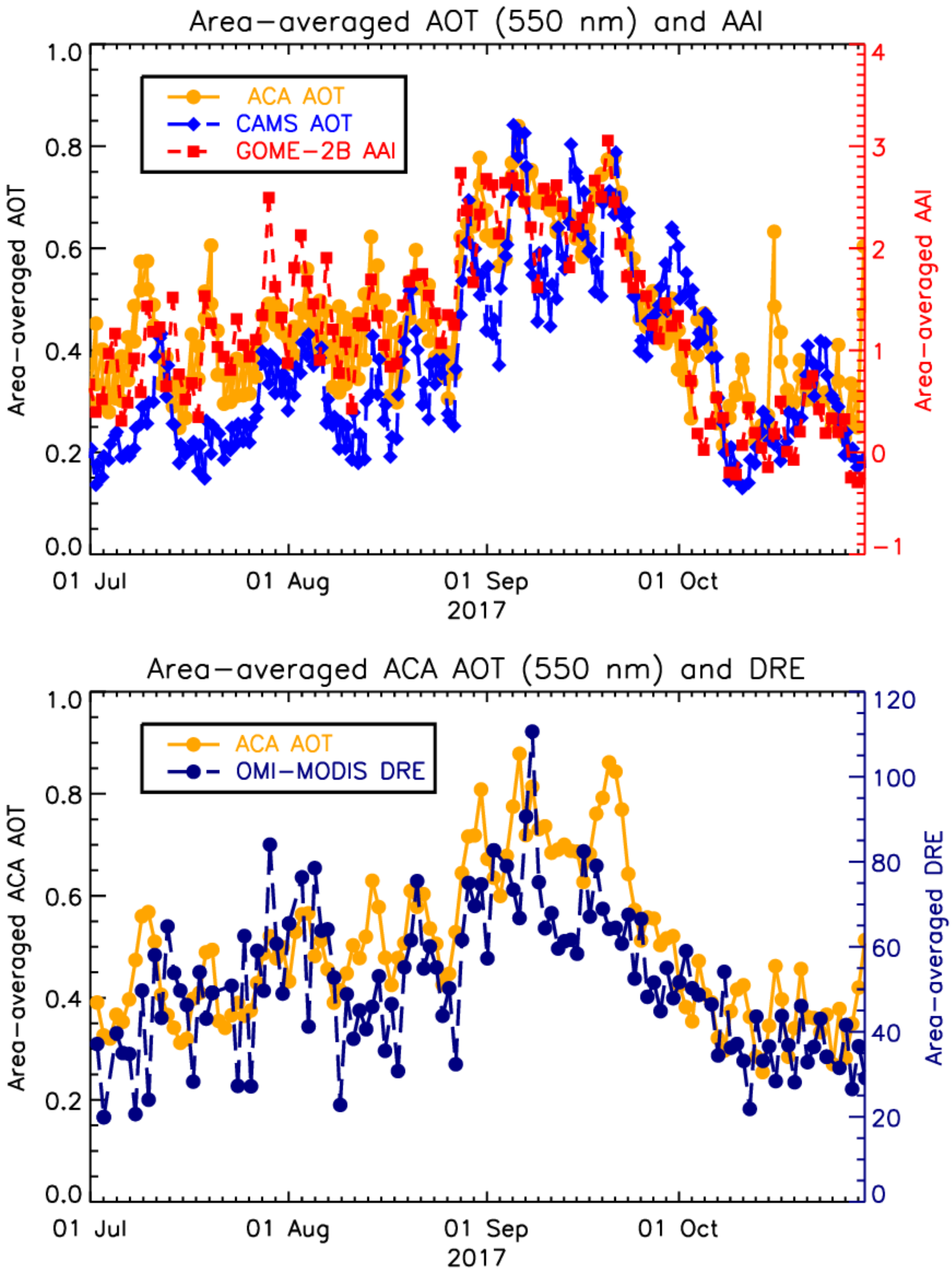

Figure 10. (top) Above-Cloud Aerosols AOT at 550 nm (orange), CAMS Total Aerosol Optical Depth at 550 nm model data (blue) and GOME-2 AAI (red) averaged over 10–20°S and 5–15°E (red rectangular area in Figure 3), from July to October 2017. The ACA AOT data were averaged each day at 09:00 and 09:30 UTC, the CAMS data ta 09:00 UTC was taken, while the AAI is available once a day around 9:30 LT. The AAI is scaled to match the AOT curves, the AAI values are indicated at the right side of the plot. (bottom) Above-Cloud Aerosols AOT at 550 nm (orange) and OMI-MODIS instantaneous Direct Radiative Effect (DRE, dark blue), averaged over 10–20°S and 5–15°E (red rectangular area in Figure 3), from July to October 2017. The ACA AOT data were averaged each day at 13:30 UTC, the DRE is available once a day around the local overpass time of OMI and MODIS around 13:30 LT.

https://doi.org/10.5194/egusphere-2026-4481
Preprint. Discussion started: 6 August 2026

AOT measurements that are only performed when clouds are present. Still, a good agreement is found between the data sets, which suggests that the observations in the clear-sky and cloudy scenes are consistent.

4.2 Comparison with GOME-2B AAI

GOME-2 are a series of UV-spectrometers onboard the MetOp satellites. AAI data at 340 and 380 nm, from GOME-2 onboard Metop-B, with an equator crossing time of 9:30 L, were also averaged over the area indicated by the red rectangle in Fig. 3. The result is shown in the top panel of Fig. 10 in red. AAI data have the advantage that they can be measured almost equally well in clear-sky and cloudy scenes (e.g. de Graaf et al., 2005) and in general higher numbers indicate increased absorption of UV-light by increased numbers of aerosols or by absorbing aerosols at a higher altitude. Fig. 10 shows a strong correlation between the GOME-2B AAI and the ACA AOT and CAMS AOT. Note that the value of the AAI is indicated on the right of the plot, and that the scaling between AAI and AOT is arbitrary, depending on calibration details of the instruments and the wavelengths for the AAI. The correlation between the AAI and the ACA AOT from SEVIRI is very high. Qualitatively, they show similar behaviour during the four months, with strongly increased values during September 2017, when the burning on the African continent peaked. In October the values decline to background values.

The AAI can thus be used to indicate the relevance of the smoke correction for cloud retrievals in the SEAO area. The biomass burning season in west Africa as inferred from the AAI time series in Fig. 10 is very persistent, as demonstrated by a synchronised AAI time series from multiple UV-spectrometers from 1978 to present, published on the Thematic Emission Monitoring Integrated Services (TEMIS) website (Tilstra et al., 2011). The AAI from the multiple sensors was averaged over the entire region shown in Fig. 3 for all years to show the average AAI and standard deviation per month, see Fig. 11. The region is affected by smoke mainly starting in June and peaking in August and September, after which the monsoonal rains set in and the fire season ends. This pattern is very persistent over the last five decades. Cloud retrievals must be considered biased when smoke plumes cover clouds during these months, and, depending on the circumstances, any month.

4.3 Comparison with instantaneous Direct Radiative Effect from OMI-MODIS measurements

The ACA AOT not only has an effect on the retrieved cloud parameters because of the reduction in reflected radiation at TOA due to the aerosols, but the reduction in radiation is also of interest by itself for climate studies. Aerosol Direct Radiative Effect (DRE), the change in radiation flux due to the presence of aerosol in the atmospheric column, is very strongly dependent on the brightness of the scene. Over dark scenes, i.e. most cloud-free scenes, scattering dominates the absorption by aerosols, even for highly absorbing aerosols. Since the amount of reflected radiation is low for a dark surface, aerosols add radiation by scattering to the TOA, resulting in a cooling of the atmosphere and the surface below. In very bright scenes on the other hand, like over clouds or snow- or ice-covered surfaces, the scattering by aerosols is negligible, and for these scenes the absorption of radiation by aerosols becomes very pronounced, especially because the amount of reflected light is large. For small particles like smoke, the amount of absorbed radiation is strongly wavelength-dependent and peaks in the UV. Consequently, the aerosols absorb radiation and add heat to the atmosphere, resulting in a warming effect. This positive DRE can be very strong, especially

https://doi.org/10.5194/egusphere-2026-4481
Preprint. Discussion started: 6 August 2026

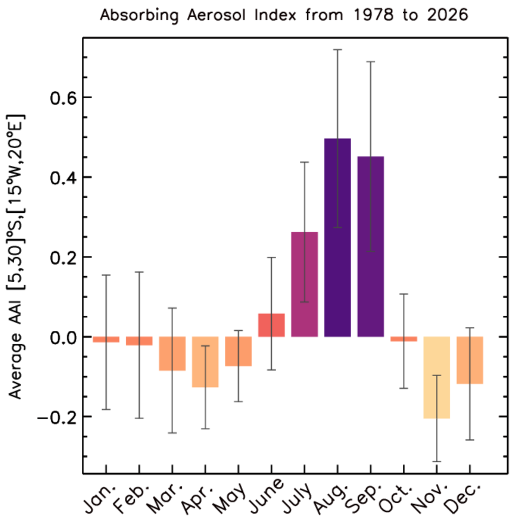

Figure 11. Absorbing Aerosol Index from TOMS, GOME-1, SCIAMACHY, OMI, GOME-2A, GOME-2B, and GOME-2C sensors, synchronised to account for wavelength and footprint differences and averaged per month between 1978 and 2026 over (15°W-15°, 5-30°S). The bars show the standard deviation of the monthly averaged AAI per month over all years.

over the SEAO (e.g. Chand et al., 2009; Peters et al., 2011; Costantino and Bréon, 2013; Meyer et al., 2013; de Graaf et al., 2012, 2014; Peers et al., 2015).

275 The ACA AOT can be related to the instantaneous aerosol DRE in cloudy scenes, using an approximate expression for the change in albedo at TOA due to an aerosol layer, $\Delta\rho$, versus the albedo of the surface underneath, given by Lenoble et al. (1982):

$$\Delta\rho = \rho - \rho_s = \mathrm{AOT}(\omega_0(1-g)(1-g)^2 - 4(1-\omega_0)\rho_s), \tag{2}$$

where ρ is the albedo at TOA and ρ_s the surface albedo. If the surface albedo is assumed to be (a constant) cloud brightness,
280 taking into account that cloud height has a very small impact on the reflectance at TOA (Ahmad et al., 2004), and neglecting the part of the AOT in clear scenes and the scattering part, Eq. 2 indicates a direct relationship between the AOT and the change in reflectance at TOA due to the aerosols, which is the aerosol DRE. In the bottom panel of Fig. 10 this is illustrated for the ACA AOT and OMI-MODIS instantaneous aerosol DRE averaged over the same red rectangular area as before. The OMI-MODIS DRE was determined from reflectance measurements of cloud scenes only (de Graaf et al., 2019). Figure 10 shows indeed a
285 strong correlation between the ACA AOT and instantaneous DRE due to aerosols in the four months of 2017 over the SEAO, with an arbitrary scaling between the two. The same temporal variation can be observed, again illustrating the strong influence of the biomass burning smoke on the clouds and the TOA radiation in this climate sensitive area.

https://doi.org/10.5194/egusphere-2026-4481
Preprint. Discussion started: 6 August 2026

5 Developments for MTG-FCI

A next step in the development of the ACA AOT retrieval will be the application to Flexible Combined Imager (FCI) measurements, which has extended capabilities compared to SEVIRI. FCI has a ten minute repeat cycle, a spatial resolution of 0.5 to 1-2 km^2, and additional spectral channels in the visible and infrared. Especially the channel at 444 nm should add additional information about aerosols (above clouds). FCI was launched in December 2022 onboard the MTG-I1 satellite, which is the first of a series of satellites to provide continuous data for weather forecasting from geostationary orbit over the next two decades.

A first test was performed of the ACA AOT retrieval using FCI measurements at the same channels as SEVIRI, to show the feasibility of the method for FCI. The above analysis for SEVIRI was repeated with FCI data on 14 August 2025, when a smoke layer from extensive annual burning over western Africa covered the stratocumulus cloud deck over the south-east Atlantic Ocean. A small section of the FCI disc was processed from 6–22°S and 6°W–7°E, comprising 1146×1472 (1.7M) pixels. In the FCI retrievals, the cloud height was set to a fixed height of 2 km. Example images of the retrieval results are shown in Fig. 12 for 11:30 UTC.

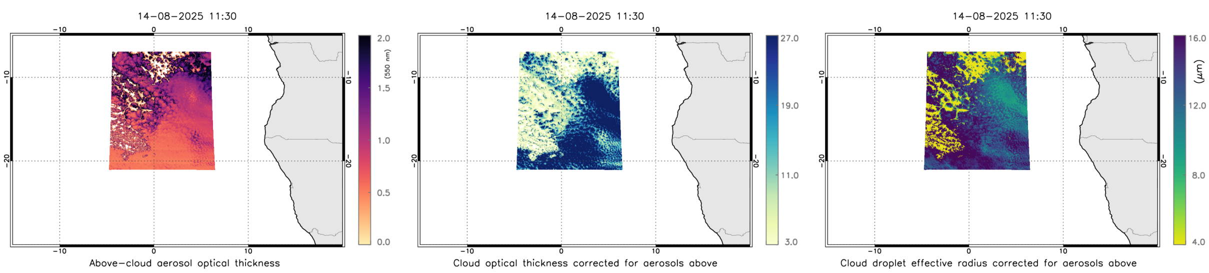

Figure 12. ACA AOT, ACA COT, and ACA CER on 14 Aug. 2025, 11:30 UTC between 6–22°S and 6°W–7°E from the FCI instrument on MTG-I1.

The diurnal cycle on 14 Aug. 2025 of the three retrieval products ACA AOT, COT and CER is shown in Fig.13, compared to the retrieval of COT and CER without aerosols considered above the clouds. Again, the latter two (named CPP retrievals) are computed with the same algorithm with AOT set to zero, as before. Figure 13 clearly shows the cloud bow and glory features around 9:30, 14:30 and noon, which are well-known retrieval artefacts. CER is affected considerably (2–3 micrometers) by the aerosol layer, and COT is clearly enhanced by it. Contrary to the CPP COT, which is relatively stable during the day, the retrieval of ACA COT is very variable, starting at a very high value of around 200 at 7:00 UTC, dropping to around 25 during mid-afternoon and rising steeply again to 120 around 16:50 UTC. The exact reason for this behaviour, also present in the SEVIRI retrievals but to a much lesser extent, has not been investigated. But apparently, the larger photon path through the aerosol layer during low sun geometries has a much stronger effect on the retrieved COT than can be represented in the plane-parallel LUT calculations. This is an effect that should be corrected when applied in operational cloud retrievals.

https://doi.org/10.5194/egusphere-2026-4481
Preprint. Discussion started: 6 August 2026

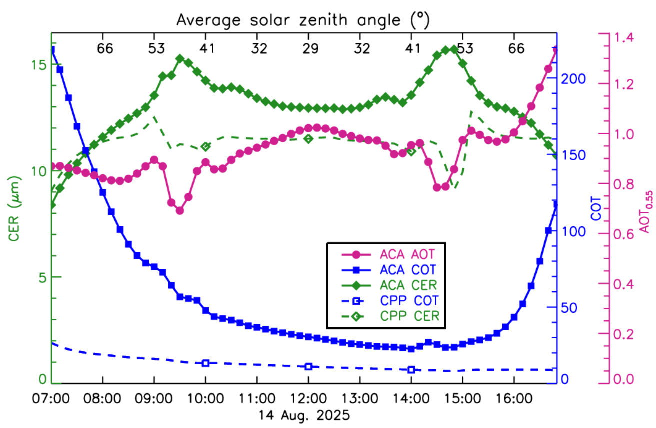

Figure 13. Diurnal cycle of the ACA AOT, COT and CER, and CPP COT and CER on 14 Aug. 2025, between 6–22°S and 6°W–7°E.

Finally, the histograms of changes to the COT and CER are shown for the FCI data in Fig. 14. All retrievals over the area shown in Fig. 12 between 10:00 and 14:00 were averaged. The mean ACA AOT at 0.55 μm for this period was 0.95. The changes are similar as those with SEVIRI data, but larger. The COT change is from 13.5 to 30.0, which is a factor 2.2 increase. The distribution shows a larger change than for SEVIRI data, from small values below 30 to a wide distribution of values up to 100 and even larger, which are not present in the CPP values. The change in CER is a 40% increase in the average value, with a shift in the distribution towards larger values, as before.

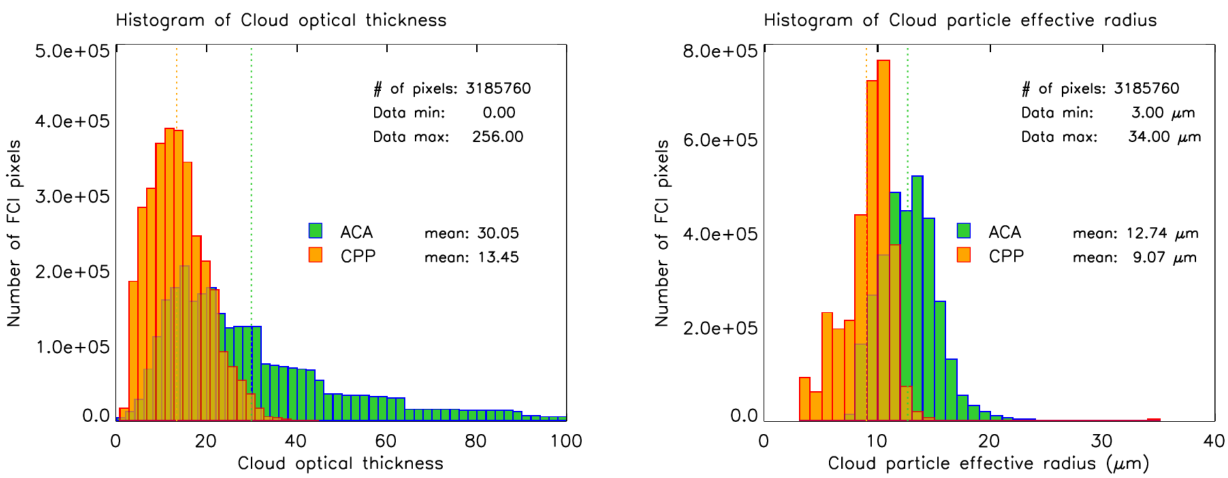

Figure 14. (Left panel) Histogram of the cloud optical thickness on 14 Aug. 2025 from 10:00–15:00, in the area between 6–22°S and 6°W–7°E, corrected for aerosols above the clouds (ACA; green) and the CPP (orange) retrievals. (Right panel) Same as the left panel but for the cloud particle effective radius.

https://doi.org/10.5194/egusphere-2026-4481
Preprint. Discussion started: 6 August 2026

6 Discussion and conclusions

Smoke from annual dry season burning in Africa, severely affects clouds over the Atlantic Ocean, which is an active research field and important for climate monitoring and global warming attribution. The semi-permanent marine stratocumulus cloud decks over the global oceans west of the continents effectively cool the climate system by reflecting incoming solar radiation over the dark ocean surface. A change in this cloud deck can have very large warming or cooling effects.

Satellite-based cloud products, such as the CLAAS-3 data record, play an important role in monitoring the variability of and changes in the distribution of cloud fields. Biases in the retrieved cloud properties should be minimised where possible. Peers et al. (2019) showed the effectiveness of an ACA AOT retrieval algorithm for smoke above clouds, meanwhile correcting the Nakajima-King COT and CER retrieval products for the reduction of reflectance in the visible channels due to absorption by the smoke. The current study quantifies the effect of the biases, which is especially large for COT. During a typical event of biomass burning in 2017, for a mean ACA AOT of around 0.82, a 1.9 times larger mean COT was observed compared to the non-corrected COT while the CER was about 40% higher. The results from the FCI measurements in 2025 show even higher biases, with the COT increased by a factor 2.2 due to smoke over the clouds and the CER increased by 40%. Both SEVIRI and FCI results show a consistent increase in both CER and COT for retrievals corrected for absorption by aerosols. Especially, the distribution of bias-corrected COT retrievals becomes very wide. This is likely partly the result of values during low sun geometries, which are not well represented in the plane-parallel LUT calculations. The ACA COT retrievals show a large, nonphysical increase in the morning and late afternoon, that should be corrected using 3D or RTM that account better for the curvature of the Earth.

The retrievals presented here were performed using an aerosol model with fixed smoke properties, like single scattering albedo, Ångström exponent and size distribution, determined as accurately as possible during an aircraft campaign in 2017. Since smoke properties vary and other absorbing aerosols may be present, like dust, the operational application of the current algorithm may introduce biases depending on aerosol type. However, these will likely be smaller than the biases due to the absence of accounting for aerosol absorption. Furthermore, in the near future, (semi-)operational or climatological information on aerosol properties may be expected from instruments like Spectro-polarimeter for Planetary Exploration one (SpexONE) (Hasekamp, 2010) on the Plankton, Aerosol, Cloud, ocean Ecosystem (PACE)mission and Earth Clouds, Aerosol and Radiation Explorer (EarthCARE) (Donovan et al., 2024). This will help improve the accuracy of the used aerosol model in the retrieval, even though the biomass burning season over Africa is very persistent and shows variability mainly from changes in large-scale circulations rather than changes in fuel type.

This study shows the clear impact of smoke on cloud optical and microphysical properties retrievals from passive VIS-SWIR imagers, which have been known since the study by Haywood et al. (2004). COT is underestimated due to visible light absorption by smoke aerosols. CER is also underestimated, in particular if a SWIR channel near 1.6 micron is used, at which cloud particles are moderately absorbing. Note that many satellite data records, including CLAAS-3, contain CER retrievals at higher SWIR wavelengths, such as 2.1, 2.2 or 3.9 micron, where clouds are more absorbing and CER biases are much smaller. Nevertheless, it is recommended to correct cloud retrievals for the presence of absorbing aerosols. Even a simple retrieval as presented here, based on one aerosol type and a simple fixed cloud model, would be helpful to better quantify the cloud parameters under aerosol-polluted circumstances and assess the quality of the retrievals.

Furthermore, FCI has excellent instrument capabilities to extend this type of retrieval further. The extra visible channel at 0.44μm is well suited to capture absorbing aerosol properties from small particles like smoke even better than at 0.64μm. As a next step, we have started to prepare an ACA AOT retrieval algorithm centred at 0.44, 0.64 and 2.25μm. The larger spectral distance between the channels will improve the retrieval accuracy and convergence rate. Additionally, the range of ACA AOT will be extended beyond 1.5 at 0.6 microns, since much thicker smoke plumes can often be observed over the SEAO.

The algorithm can also be applied to TROPOMI and Sentinel-5 measurements, which are spectrometers that measure from the UV to the SWIR. The application of the algorithm for these instruments will be attempted at 0.354, 0.670 and 2.314μm, still further increasing the spectral distance between the channels and increasing the sensitivity to aerosol absorption at UV wavelengths. An additional advantage is the high spectral resolution of the spectrometers. The chosen channels can be very narrow (like 1 nm) to avoid gaseous absorption bands, which makes the atmospheric correction trivial and less critical.

Data availability. SEVIRI data is freely available on (Meirink et al., 2022)

Author contributions. MdG implemented the ACA retrieval, performed the analysis and wrote the paper, PW created the LUT and advised, NB participated in the CLAAS-3 CPP retrievals, reviewed and edited the paper, JFM supervised the project.

Competing interests. The authors declare that they have no conflict of interest.

Acknowledgements. This work was funded as a federated activity of the Atmospheric Composition (AC) SAF and CM SAF of EUMETSAT, project Above-Cloud Aerosol Cases: Improved Assessment from SEVIRI (ACACIAS), CM-AC_FA20_01.

https://doi.org/10.5194/egusphere-2026-4481
Preprint. Discussion started: 6 August 2026

References

Ahmad, Z., Bhartia, P. K., and Krotkov, N.: Spectral properties of backscattered UV radiation in cloudy atmospheres, J. Geophys. Res., 109, D01201, https://doi.org/10.1029/2003JD003395, 2004.

Ajoku, O. F., Miller, A. J., and Norris, J. R.: Impacts of aerosols produced by biomass burning on the stratocumulus-to-cumulus transition in the equatorial Atlantic, Atmos. Sci. Lett., 22, e1025, https://doi.org/https://doi.org/10.1002/asl.1025, 2021.

Albrecht, B. A., Randall, D. A., and Nicholls, S.: Observations of Marine Stratocumulus Clouds During FIRE, Bull. Am. Meteor. Soc., 69, 618–626, 1988.

Benas, N., Finkensieper, S., Stengel, M., van Zadelhoff, G.-J., Hanschmann, T., Hollmann, R., and Meirink, J. F.: The MSG-SEVIRI-based cloud property data record CLAAS-2, Earth System Science Data, 9, 415–434, https://doi.org/10.5194/essd-9-415-2017, 2017.

Benas, N., Meirink, J. F., Stengel, M., and Stammes, P.: Sensitivity of liquid cloud optical thickness and effective radius retrievals to cloud bow and glory conditions using two SEVIRI imagers, Atmos. Meas. Tech. Disc., 2019, 1–25, https://doi.org/10.5194/amt-2018-439, 2019.

Benas, N., Solodovnik, I., Stengel, M., Hüser, I., Karlsson, K.-G., Håkansson, N., Johansson, E., Eliasson, S., Schröder, M., Hollmann, R., and Meirink, J. F.: CLAAS-3: the third edition of the CM SAF cloud data record based on SEVIRI observations, Earth System Sci. Data, 15, 5153–5170, https://doi.org/10.5194/essd-15-5153-2023, 2023.

Bretherton, C. S. and Wyant, M. C.: Moisture Transport, Lower-Tropospheric Stability, and Decoupling of Cloud-Topped Boundary Layers, J. Atmos. Sci., 54, 148 – 167, https://doi.org/10.1175/1520-0469(1997)054<0148:MTLTSA>2.0.CO;2, 1997.

Chand, D., Wood, R., Anderson, T. L., Satheesh, S. K., and Charlson, R. J.: Satellite-derived direct radiative effect of aerosols dependent on cloud cover, Nat. Geosci., 2, https://doi.org/10.1038/NGEO437, 2009.

Costantino, L. and Bréon, F.-M.: Satellite-based estimate of aerosol direct radiative effect over the South-East Atlantic, Atmospheric Chemistry and Physics Discussions, 13, 23 295–23 324, https://doi.org/10.5194/acpd-13-23295-2013, 2013.

de Graaf, M., Stammes, P., Torres, O., and Koelemeijer, R. B. A.: Absorbing Aerosol Index: Sensitivity Analysis, application to GOME and comparison with TOMS, J. Geophys. Res., 110, D01201, https://doi.org/10.1029/2004JD005178, 2005.

de Graaf, M., Tilstra, L. G., Aben, I., and Stammes, P.: Satellite observations of the seasonal cycles of absorbing aerosols in Africa related to the monsoon rainfall, 1995 - 2008., Atmos. Environ., 44, 1274–1283, https://doi.org/10.1016/j.atmosenv.2009.12.038, 2010.

de Graaf, M., Tilstra, L. G., Wang, P., and Stammes, P.: Retrieval of the aerosol direct radiative effect over clouds from spaceborne spectrometry, J. Geophys. Res., 117, https://doi.org/10.1029/2011JD017160, 2012.

de Graaf, M., Bellouin, N., Tilstra, L. G., Haywood, J., and Stammes, P.: Aerosol direct radiative effect of smoke over clouds over the southeast Atlantic Ocean from 2006 to 2009, Geophys. Res. Lett., 41, 7723–7730, https://doi.org/10.1002/2014GL061103, 2014.

de Graaf, M., Tilstra, L., and Stammes, P.: Aerosol direct radiative effect over clouds from synergic OMI and MODIS reflectances, Atmos. Meas. Tech., 2019, 5119 – 5135, https://doi.org/10.5194/amt-12-5119-2019, 2019.

De Haan, J. F., Bosma, P. B., and Hovenier, J. W.: The adding method for multiple scattering calculations of polarized light, Astron. Astrophys., 183, 371–391, 1987.

Diamond, M. S., Dobracki, A., Freitag, S., Small Griswold, J. D., Heikkila, A., Howell, S. G., Kacarab, M. E., Podolske, J. R., Saide, P. E., and Wood, R.: Time-dependent entrainment of smoke presents an observational challenge for assessing aerosol–cloud interactions over the southeast Atlantic Ocean, Atmos. Chem. Phys., 18, 14 623–14 636, https://doi.org/10.5194/acp-18-14623-2018, 2018.

Donovan, D. P., van Zadelhoff, G.-J., and Wang, P.: The EarthCARE lidar cloud and aerosol profile processor (A-PRO): the A-AER, A-EBD, A-TC, and A-ICE products, Atmos. Meas. Tech., 17, 5301–5340, https://doi.org/10.5194/amt-17-5301-2024, 2024.

https://doi.org/10.5194/egusphere-2026-4481
Preprint. Discussion started: 6 August 2026

Forster, P., Storelvmo, T., Armour, K., Collins, W., Dufresne, J.-L., Frame, D., Lunt, D., Mauritsen, T., Palmer, M., Watanabe, M., Wild, M., , and Zhang, H.: The Earth's Energy Budget, Climate Feedbacks and Climate Sensitivity, pp. 923–1054, Cambridge University Press, https://doi.org/10.1017/9781009157896.009, 2023.

Garstang, M., Tyson, P. D., Swap, R., Edwards, M., Kållberg, P., and Lindesay, J. A.: Horizontal and vertical transport of air over southern Africa, J. Geophys. Res., 101, D19, 1996.

Hasekamp, O. P.: Capability of multi-viewing-angle photo-polarimetric measurements for the simultaneous retrieval of aerosol and cloud properties, Atmos. Meas. Tech., 3, 839–851, https://doi.org/10.5194/amt-3-839-2010, 2010.

Haywood, J. M., Osborne, S. R., and Abel, S. J.: The effect of overlying absorbing aerosol layers on remote sensing retrievals of cloud effective radius and cloud optical depth, Q. J. R. Meteorol. Soc., 130, 779–800, https://doi.org/10.1256/qj.03.100, 2004.

Haywood, J. M., Abel, S. J., Barrett, P. A., Bellouin, N., Blyth, A., Bower, K. N., Brooks, M., Carslaw, K., Che, H., Coe, H., Cotterell, M. I., Crawford, I., Cui, Z., Davies, N., Dingley, B., Field, P., Formenti, P., Gordon, H., de Graaf, M., Herbert, R., Johnson, B., Jones, A. C., Langridge, J. M., Malavelle, F., Partridge, D. G., Peers, F., Redemann, J., Stier, P., Szpek, K., Taylor, J. W., Watson-Parris, D., Wood, R., Wu, H., and Zuidema, P.: The CLoud–Aerosol–Radiation Interaction and Forcing: Year 2017 (CLARIFY-2017) measurement campaign, Atmospheric Chemistry and Physics, 21, 1049–1084, https://doi.org/10.5194/acp-21-1049-2021, 2021.

Johnson, B. T., Shine, K. P., and Forster, P. M.: The semi–direct aerosol effect: Impact of absorbing aerosols on marine stratocumulus, Q. J. R. Meteorol. Soc., 130, 1407–1422, https://doi.org/10.1256/qj.03.61, 2004.

Keil, A. and Haywood, J. M.: Solar radiative forcing by biomass burning aerosol particles during SAFARI 2000: A case study based on measured aerosol and cloud properties, J. Geophys. Res., 108, D13, https://doi.org/10.1029/2002JD002315, 2003.

Lenoble, J., Tanré, D., Deschamps, P. Y., and Herman, M.: A Simple Method to Compute the Change in Earth-Atmosphere Radiative Balance Due to a Stratospheric Aerosol Layer, J. Atmos. Sci., 39, 2565–2576, https://doi.org/10.1175/1520-0469(1982)039<2565:ASMTCT>2.0.CO;2, 1982.

Meirink, J. F., Roebeling, R. A., and Stammes, P.: Inter-calibration of polar imager solar channels using SEVIRI, Atmos. Meas. Tech., 6, 2495–2508, https://doi.org/10.5194/amt-6-2495-2013, 2013.

Meirink, J. F., Karlsson, K.-G., Solodovnik, I., Hüser, I., Benas, N., Johansson, E., Håkansson, N., Stengel, M., Selbach, N., Marc, S., and Hollmann, R.: CLAAS-3: CM SAF CLoud property dAtAset using SEVIRI - Edition 3, https://doi.org/10.5676/EUM_SAF_CM/CLAAS/V003, 2022.

Meyer, K., Platnick, S., Oreopoulos, L., and Lee, D.: Estimating the direct radiative effect of absorbing aerosols overlying marine boundary layer clouds in the southeast Atlantic using MODIS and CALIOP, J. Geophys. Res., 118, 4801–4815, https://doi.org/10.1002/jgrd.50449, 2013.

Myhre, G., Samset, B. H., Schulz, M., Balkanski, Y., Bauer, S., Berntsen, T. K., Bian, H., Bellouin, N., Chin, M., Diehl, T., Easter, R. C., Feichter, J., Ghan, S. J., Hauglustaine, D., Iversen, T., Kinne, S., Kirkevåg, A., Lamarque, J.-F., Lin, G., Liu, X., Lund, M. T., Luo, G., Ma, X., van Noije, T., Penner, J. E., Rasch, P. J., Ruiz, A., Seland, Ø., Skeie, R. B., Stier, P., Takemura, T., Tsigaridis, K., Wang, P., Wang, Z., Xu, L., Yu, H., Yu, F., Yoon, J.-H., Zhang, K., Zhang, H., and Zhou, C.: Radiative forcing of the direct aerosol effect from AeroCom Phase II simulations, Atmos. Chem. Phys., 13, 1853–1877, https://doi.org/10.5194/acp-13-1853-2013, 2013.

Nakajima, T. and King, M. D.: Determination of the Optical Thickness and Effective Particle Radius of Clouds from Reflected Solar Radiation Measurements: Part I: Theory, J. Atmos. Sci., 47, 1878–1893, https://doi.org/10.1175/1520-0469(1990)047<1878:DOTOTA>2.0.CO;2, 1990.

https://doi.org/10.5194/egusphere-2026-4481
Preprint. Discussion started: 6 August 2026

Painemal, D., Kato, S., and Minnis, P.: Boundary layer regulation in the southeast Atlantic cloud microphysics during the biomass burning season as seen by the A-train satellite constellation, Journal of Geophysical Research: Atmospheres, 119, 11,288–11,302, https://doi.org/10.1002/2014JD022182, 2014.

Paluch, I. R. and Lenschow, D. H.: Stratiform Cloud Formation in the Marine Boundary Layer, J. Atmos. Sci., 48, 2141 – 2158, https://doi.org/10.1175/1520-0469(1991)048<2141:SCFITM>2.0.CO;2, 1991.

Peers, F., Waquet, F., Cornet, C., Dubuisson, P., Ducos, F., Goloub, P., Szczap, F., Tanré, D., and Thieuleux, F.: Absorption of aerosols above clouds from POLDER/PARASOL measurements and estimation of their direct radiative effects, Atmos. Chem. Phys., 15, 4179–4196, https://doi.org/10.5194/acp-15-4179-2015, 2015.

Peers, F., Francis, P., Fox, C., Abel, S. J., Szpek, K., Cotterell, M. I., Davies, N. W., Langridge, J. M., Meyer, K. G., Platnick, S. E., and Haywood, J. M.: Observation of absorbing aerosols above clouds over the south-east Atlantic Ocean from the geostationary satellite SEVIRI – Part 1: Method description and sensitivity, Atmos. Chem. Phys., 19, 9595–9611, https://doi.org/10.5194/acp-19-9595-2019, 2019.

Peters, K., Quaas, J., and Bellouin, N.: Effects of absorbing aerosols in cloudy skies: a satellite study over the Atlantic Ocean, Atmos. Chem. Phys., 11, 1393–1404, https://doi.org/10.5194/acp-11-1393-2011, 2011.

Rajapakshe, C., Zhang, Z., Yorks, J. E., Yu, H., Tan, Q., Meyer, K., Platnick, S., and Winker, D. M.: Seasonally transported aerosol layers over southeast Atlantic are closer to underlying clouds than previously reported, Geophys. Res. Lett., 44, 5818–5825, https://doi.org/https://doi.org/10.1002/2017GL073559, 2017.

Randall, D. A., Coakley, J. A., Lenschow, D. H., Fairall, C. W., and Kropfli, R. A.: Outlook for research on subtropical marine stratiform clouds, Bull. Am. Meteor. Soc., 65, 1290–1301, https://doi.org/10.1175/1520-0477(1984)065<1290:Ofrosm>2.0.Co;2, 1984.

Redemann, J., Wood, R., Zuidema, P., Doherty, S. J., Luna, B., LeBlanc, S. E., Diamond, M. S., Shinozuka, Y., Chang, I. Y., Ueyama, R., Pfister, L., Ryoo, J., Dobracki, A. N., da Silva, A. M., Longo, K. M., Kacenelenbogen, M. S., Flynn, C. J., Pistone, K., Knox, N. M., Piketh, S. J., Haywood, J. M., Formenti, P., Mallet, M., Stier, P., Ackerman, A. S., Bauer, S. E., Fridlind, A. M., Carmichael, G. R., Saide, P. E., Ferrada, G. A., Howell, S. G., Freitag, S., Cairns, B., Holben, B. N., Knobelspiesse, K. D., Tanelli, S., L'Ecuyer, T. S., Dzambo, A. M., Sy, O. O., McFarquhar, G. M., Poellot, M. R., Gupta, S., O'Brien, J. R., Nenes, A., Kacarab, M. E., Wong, J. P. S., Small-Griswold, J. D., Thornhill, K. L., Noone, D., Podolske, J. R., Schmidt, K. S., Pilewskie, P., Chen, H., Cochrane, S. P., Sedlacek, A. J., Lang, T. J., Stith, E., Segal-Rozenhaimer, M., Ferrare, R. A., Burton, S. P., Hostetler, C. A., Diner, D. J., Platnick, S. E., Myers, J. S., Meyer, K. G., Spangenberg, D. A., Maring, H., and Gao, L.: An overview of the ORACLES (ObseRvations of Aerosols above CLouds and their intEractionS) project: aerosol-cloud-radiation interactions in the Southeast Atlantic basin, Atmos. Chem. Phys. Disc., 2020, 1–82, https://doi.org/10.5194/acp-2020-449, 2020.

Segelstein, D. J.: The complex refractive index of water, Msc thesis, University of Kansas City and University of Missouri, http://hdl.handle.net/10355/11599, 1981.

Stammes, P.: Spectral radiance modelling in the UV-visible range, in: IRS 2000: Current problems in atmospheric radiation, edited by Smith, W. and Timofeyev, Y., pp. 385–388, A. Deepak Publishing, Hampton (VA), 2001.

Stengel, M., Kniffka, A., Meirink, J. F., Lockhoff, M., Tan, J., and Hollmann, R.: CLAAS: the CM SAF cloud property data set using SEVIRI, Atmos. Chem. Phys., 14, 4297–4311, https://doi.org/10.5194/acp-14-4297-2014, 2014.

Stevens, B.: ATMOSPHERIC MOIST CONVECTION, Annual Review of Earth and Planetary Sciences, 33, 605–643, https://doi.org/https://doi.org/10.1146/annurev.earth.33.092203.122658, 2005.

https://doi.org/10.5194/egusphere-2026-4481
Preprint. Discussion started: 6 August 2026

Swap, R., Garstang, M., Macko, S. A., Tyson, P. D., Maenhaut, W., Artaxo, P., Kållberg, P., and Talbot, R.: The long-range transport of southern African aerosols to the tropical South Atlantic, J. Geophys. Res., 101, D19, https://doi.org/10.1029/95JD01049, 1996.

Tilstra, L. G., de Graaf, M., Tuinder, O. N. E., van der A, R. J., and Stammes, P.: Studying trends in aerosol presence using the Absorbing Aerosol Index derived from GOME-1, SCIAMACHY, and GOME-2, in: Proceedings of the 2011 EUMETSAT Meteorological Satellite Conference, EUMETSAT, 2011.

Twomey, S. A.: The Influence of Pollution on the Shortwave Albedo of Clouds, J. Atmos. Sci., 34, 1149–1152, 1977.

Wyant, M. C., Bretherton, C. S., Rand, H. A., and Stevens, D. E.: Numerical Simulations and a Conceptual Model of the Stratocumulus to Trade Cumulus Transition, J. Atmos. Sci., 54, 168 – 192, https://doi.org/10.1175/1520-0469(1997)054<0168:NSAACM>2.0.CO;2, 1997.

Xue, H. and Feingold, G.: Large-Eddy Simulations of Trade Wind Cumuli: Investigation of Aerosol Indirect Effects, J. Atmos. Sci., 63, 1605–1622, https://doi.org/10.1175/JAS3706.1, 2006.

Yamaguchi, T., Feingold, G., Kazil, J., and McComiskey, A.: Stratocumulus to cumulus transition in the presence of elevated smoke layers, Geophys. Res. Lett., 42, 10,478–10,485, https://doi.org/https://doi.org/10.1002/2015GL066544, 2015.

Zhou, X., Ackerman, A. S., Fridlind, A. M., Wood, R., and Kollias, P.: Impacts of solar-absorbing aerosol layers on the transition of stratocumulus to trade cumulus clouds, Atmos. Chem. Phys., 17, 12 725–12 742, https://doi.org/10.5194/acp-17-12725-2017, 2017.

Zuidema, P., Sedlacek III, A. J., Flynn, C., Springston, S., Delgadillo, R., Zhang, J., Aiken, A. C., Koontz, A., and Muradyan, P.: The Ascension Island Boundary Layer in the Remote Southeast Atlantic is Often Smoky, Geophys. Res. Lett., 45, 4456–4465, https://doi.org/10.1002/2017GL076926, 2018.